Suarez, N.; Arribas Viana, MDLD.; Moreno, A.; Martinez Feliu, A. (2020). High-performing Ir- and Pt-containing catalysts based on mesoporous beta zeolite for the selective ring opening of decalin. Catalysis Science & Technology. 10(4):1073-1085. https://doi.org/10.1039/c9cy01812c

ARTICLE

High-performing Ir- and Pt-containing catalysts based on mesoporous beta zeolite for the selective ring opening of decalin

Received 00th January 20xx,
Accepted 00th January 20xx

DOI: 10.1039/x0xx00000x

Natalia Suárez,[a,b] María A. Arribas,[a] Andrés Moreno [b] and Agustín Martínez *[a]

Selective ring opening (SRO) of naphthenic molecules resulting from the hydrogenation of polyaromatics is a desirable catalytic route for upgrading low-quality diesel fractions such as hydrotreated light cycle oil (LCO) produced in catalytic crackers. In this work, catalysts based on either Ir or Pt (~ 3 wt%) dispersed on a Cs^+-exchanged mesoporous beta zeolite (β-meso) obtained by controlled desilication of a commercial beta sample (β-com, Si/Al = 19) with NaOH in presence of CTAB surfactant were prepared and evaluated for the SRO of decalin as a model reactant. In comparison to an equivalent Ir catalyst based on the commercial zeolite (Ir/Cs-β-com), the Ir catalyst based on mesoporous beta (Ir/Cs-β-meso) attained higher decalin conversions and yields of target ring opening products (C_{10}-alkylcycloalkanes, ROP, and C_{10}-alkanes or open chain decanes, OCD). An unprecedented maximum combined yield of ROP+OCD of 72.6 wt% was achieved over the Ir/Cs-β-meso catalyst at 89.2% decalin conversion. The improved catalytic performance exhibited by the catalyst based on mesoporous beta zeolite can be mainly ascribed to an increased accessibility of decalin molecules to the active sites and to a faster diffusion of ring opening products, retarding their further conversion into unwanted lighter (C_{9-}) hydrocarbons. On the other hand, the catalyst based on Pt dispersed on Cs-β-meso was less active and achieved a lower maximum combined yield of ROP+OCD (59.6 wt% at 92.7% conversion) than its homologous catalyst based on Ir. However, compared to the Ir catalyst, less branched ROP and OCD isomers (hence, more desirable from the viewpoint of cetane) were formed on the Pt catalyst. The molecular structure of main ROP and OCD isomers, as assessed by GCxGC, and the carbon number distribution of C_{9-} products indicated that cleavage of C-C bonds on the Ir-based catalysts predominantly occurred at Ir centers via the (non-selective) dicarbene hydrogenolysis mechanism. Differently, both the hydrogenolysis (via the multiplet or selective mechanism) and the bifunctional (via carbocations) pathways contributed to the breaking of C-C bonds on the Pt-based mesoporous catalyst.

1. Introduction

Hydrogenation of polycyclic aromatics followed by the selective ring opening (SRO) of the produced naphthenic compounds has been proposed as an attractive, albeit challenging, strategy for upgrading poor-quality aromatic-rich middle distillate fractions such as the LCO (Light Cycle Oil), abundantly produced in FCC units, into diesel fuel with enhanced cetane number and reduced harmful emissions [1-3]. As an additional advantage, reducing the concentration of naphthenic rings in the fuel via SRO lowers its density increasing thereby the volume of marketable fuel.

Opening of naphthenic molecules can proceed through different pathways depending on the nature of active sites involved: a) monofunctional acid catalysis on Brønsted acid sites, b) monofunctional hydrogenolysis on metal sites, and c) bifunctional catalysis involving both acid and metal sites [3-4]. Although protonic (i.e., H-form) zeolites possessing relatively strong Brønsted acid sites are active for breaking endocyclic C-C bonds in naphthenic rings via the monofunctional acid route, the final yield and selectivity of target ring opening products (ROP) are low due to excessive cracking into lighter compounds and progressive deactivation of the catalyst by coking [5]. On the other hand, some noble metals like Pd, Pt, Ir, Rh, and Ru are known to exhibit high activity for opening naphthenic rings in presence of hydrogen through a monofunctional hydrogenolysis route [3]. In this case, the prevailing hydrogenolysis mechanism, which eventually determines the molecular structure (hence, the cetane number) of the formed ROP may vary depending on the specific metal catalyst and metal properties such as particle size [2-3]. A main drawback of the monofunctional hydrogenolysis pathway is, however, the much lower reactivity of the noble metal towards opening C_6 naphthenic rings (formed by hydrogenation of aromatics) compared to C_5 rings. As originally reported by McVicker et al. [3], this issue may be overcome by combining the hydrogenolysis metal catalyst with a moderately acidic component such as amorphous silica-alumina or dealuminated large pore zeolite to promote the C_6-to-C_5 ring contraction (isomerization) prior the SRO step. Finally,

[a] *Instituto de Tecnología Química, Universitat Politècnica de València - Consejo Superior de Investigaciones Científicas (UPV-CSIC), Avda. de los Naranjos s/n, 46022 Valencia, Spain.*
[b] *Química de Recursos Energéticos y Medio Ambiente, Instituto de Química, Facultad de Ciencias Exactas y Naturales, Universidad de Antioquia UdeA, Calle 70 No.52-21, Medellín, Colombia.*
** Corresponding author: amart@itq.upv.es (A. Martínez).*

opening of naphthenic rings may also occur through a bifunctional route using catalysts on which the hydrogenolysis function (commonly Pt, Ir, or combinations thereof) is dispersed on large pore FAU (X, Y) or BEA type zeolites containing Brønsted acid sites [4]. In order to maximize the yield of the desired ROP, the catalytic functions in the bifunctional metal/zeolite catalysts need to be finely tuned to promote the C_6-to-C_5 ring isomerization on the zeolite acid sites and the subsequent SRO via hydrogenolysis on the metal sites while preventing unselective ring opening via acid catalysis. Following this strategy, researchers at Eni developed the so-coined HIPEROC (High Performance Ring Opening Catalysts) systems, on which the hydrogenolysis metal (Pt or Ir) is dispersed, typically via ionic exchange in concentrations of around 3 wt%, on faujasite or beta zeolites having most of their Brønsted acid sites neutralized by alkali cations [6]. In experiments using decalin as model naphthenic feed, such HIPEROC systems achieved high yields of ring opening products, particularly to the highest cetane open chain decanes (OCD, comprising both linear and branched C_{10} alkanes) in yields exceeding 25% [6]. Among the HIPEROC catalysts, that based on zeolite beta (Si/Al = 14) exchanged with Cs^+ cations and subsequently loaded, via ionic exchange, with 3.4 wt% Ir attained the best results, with a combined maximum yield of ROP+OCD of 59% and yield of OCD as high as 44% [6].

In earlier works, we showed that the diffusion of C_{10}-alkylcyclohexanes, typical ROP formed upon opening one of the two C_6 naphthenic rings of decalin, is significantly limited in the micropores (particularly in the smaller ones) of zeolite beta, as supported by molecular-docking simulations [7]. The enhanced diffusion limitation for some of the ring opening products formed from two-ring naphthenes (e.g., decalin and its alkyl derivatives) in bifunctional Pt/beta catalysts promoted their consecutive cracking on the zeolite acid sites resulting in lower yields of ROP compared to equivalent catalysts based on other large pore 3D zeolites like USY and ITQ-21 [8]. Moreover, diffusional restrictions in purely microporous zeolites are anticipated to become even more relevant in the SRO of bulkier naphthenes present in real feeds as in hydrotreated LCO. Bifunctional catalysts based on noble metals dispersed on acidic MCM- and SBA-type materials comprising uniformly sized mesopores and weaker Brønsted acid sites than zeolites have been explored in the SRO of multi-ring aromatic and naphthenic molecules, although with limited success. For instance, the maximum yield of ROP achieved in the SRO of decalin over a Pt-Ir/Zr-MCM-41 (atomic Si/Zr ratio= 5) catalyst with optimal metal composition (1.5 wt% Ir and 0.75 wt% Pt) was ca. 16 wt% (ROP selectivity of 26 wt%) [9], which is remarkably lower than that reported for zeolite-based HIPEROC systems.

An effective strategy to alleviate accessibility and diffusional issues in zeolite-catalyzed reactions involving bulky molecules relies on the generation of a secondary mesoporous network through controlled desilication under alkaline conditions [10-13]. For instance, a simple desilication treatment with aqueous NaOH solutions is often applied to introduce mesoporosity within the crystallites of zeolites with different topology, albeit at the cost of a certain loss of material, crystallinity, microporosity, and acidity [10, 14]. These drawbacks can be minimized by replacing NaOH with tetraalkylammonium hydroxides (e.g., TPAOH or TBAOH) or by using mixtures of NaOH and alkylammonium hydroxides [11, 15-16]. An interesting post-synthetic strategy initially developed by García-Martínez and co-workers for introducing well-controlled mesoporosity into Y zeolite crystals in a single-step process involves the use of cationic surfactants such as cetyltrimethylammonium bromide (CTAB) or chloride (CTACl) that promote the reassembly of dissolved zeolite species [17]. Moreover, desilication in alkaline solutions (e.g., NaOH, NH_4OH) combined with the addition of CTA^+ cations enables the generation of mesopores upon removal of the template while largely preserving the original zeolite properties [18-19].

Due to their enhanced mass transport and accessibility to active sites with respect to conventional zeolites, mesoporous zeolites generally display improved activity and/or selectivity as well as a lower coking rate in catalytic reactions involving bulky reactants and/or products [20-26]. The catalytic performance of such hierarchical micro-mesoporous zeolites in the SRO of multi-ring naphthenic molecules, however, has been scarcely investigated. For instance, sulfided NiW supported on a mesoporous Y zeolite, prepared by hydrothermal treatment at 150 °C for 20 h of a commercial USY (CVB720) in presence of a mixture of CTAB and TMAOH solutions, achieved higher yields of ROP in the hydrogenation and SRO of naphthalene [27] and phenanthrene [28] compared to equivalent catalysts supported on untreated USY. In both cases, the improved ROP yields upon introduction of additional mesoporosity was attributed to the easier accessibility of the bulky aromatic reactants to the active sites within the intraporous zeolite voids.

In this work, we report the advantages of introducing mesopores in zeolite beta via surfactant-assisted desilication in improving the yield and selectivity of ring opening products in the SRO of decalin on bifunctional low-acidic Ir(Pt)/Cs-beta catalysts (3 wt% metal). It will be shown that the Ir catalyst dispersed on mesoporous beta achieved an unprecedented high maximum combined yield of ring opening products (ROP+OCD) of ca. 73 wt% at 89% decalin conversion (~82 wt% selectivity), exceeding the maximum yields reported for similar HIPEROC systems based on conventional (purely microporous) zeolites. Moreover, compared with an analogous Ir catalyst dispersed on commercial zeolite beta, the catalyst based on mesoporous beta showed an enhanced yield and selectivity of high cetane OCD products due to their faster diffusion out of the zeolite pores limiting undesired consecutive reactions.

2. Experimental section

2.1. Preparation of mesoporous beta zeolite

Mesoporous zeolite beta (denoted as β-meso) was prepared from a commercial beta sample (CP814C, Si/Al= 19, NH_4^+-form, Zeolyst International, designated as β-com) through controlled surfactant-assisted desilication following the procedure reported in a recent study by some of the co-authors of the present work [19]. In brief, 5.0 g of commercial beta were added to 31.5 cm^3 of an aqueous solution on which 0.46 g of NaOH (Scharlau, 98%) and 2.5 g of cetyltrimethylammonium bromide (CTAB, Sigma-Aldrich, ≥ 98%) were previously dissolved. The mixture was magnetically agitated at room temperature for 20 min, transferred to a Teflon-lined stainless-steel autoclave, and heated at 80 °C for 6 h. Subsequently, the solid was filtered, washed with deionized water, and dried at 60 °C overnight. The final material was obtained after removal of the

surfactant by thermal treatment at 550 °C (heating rate of 3 °C/min) in flowing N_2 for 1 h and then in air for 6 h at the same temperature.

2.2. Preparation of Ir(Pt)/Cs-beta catalysts

Prior incorporation of the metal (Ir, Pt), the calcined (H-form) mesoporous beta sample was submitted to two consecutive ionic exchanges with, respectively, Na^+ and Cs^+ solutions in order to reduce the density of Brønsted acid sites. First, the zeolite was exchanged with a 1M aqueous solution of $NaNO_3$ (Fluka, ≥99%) at 80 °C for 4 h, filtered, washed with deionized water, and dried at 80 °C for 12 h. Then, the Na-beta sample was subjected to a second ionic exchange with a 0.1M aqueous solution of CsCl (Fisher Scientific, ≥99.99%) at the same conditions applied in the previous exchange with Na^+ cations. The alkali-exchanged mesoporous beta zeolite is denoted hereafter as Cs-β-meso.

Two catalysts were then prepared by introducing either Ir or Pt as hydrogenolysis function via ionic exchange (80 °C, 2 h) of the Cs-β-meso sample with aqueous solutions of $[Ir(NH_3)_5Cl]Cl_2$ (Sigma-Aldrich, 99.95%) or $Pt(NH_3)_4(NO_3)_2$ (Sigma-Aldrich, 99.99%) precursors, respectively, targeting in both cases a nominal metal content of 3 wt%. After incorporation of the metal function, the samples were dried at 80 °C for 12 h and then calcined at 300 °C for 2 h under a high air flowrate of 1 L/(g_{cat}·min) and slow ramping of 0.2 °C/min in order to prevent extensive metal sintering. The calcined Ir- and Pt-loaded catalysts are labelled as Ir/Cs-β-meso and Pt/Cs-β-meso, respectively. For comparison purposes, an additional catalyst was obtained by loading Ir (3 wt% nominal content) through ionic exchange on the commercial beta sample pre-exchanged with Na^+ and then with Cs^+ cations (Cs-β-com), followed by washing, drying, and calcination under the same experimental conditions applied for the preparation of Ir/Cs-β-meso. The Ir catalyst based on the commercial beta is hereafter termed as Ir/Cs-β-com.

2.3. Characterization techniques

The bulk Si/Al ratio and alkali (Na, Cs) content in the zeolites and catalysts were determined by inductively coupled plasma-optical emission spectrometry (ICP-OES) in a Varian 715-ES spectrometer after dissolution of the solids in an acid mixture of HNO_3: HF: HCl in a 1:1:3 volume ratio. The concentration of metal (Ir, Pt) in the calcined catalysts was determined by energy-dispersive X-ray spectroscopy (EDX) using a microprobe (INCA PentaFETx3 Oxford Instruments) implemented in a field emission scanning electron microscope (FESEM, JEOL JSM 6490 LC microscope).

X-ray powder diffraction (XRD) patterns were recorded on a Philips X'Pert diffractometer equipped with a PANanalytical X'Celerator detector and using monochromatic Cu K_α radiation (λ_1= 0.15406 nm, λ_2= 0.15444 nm, I_2/I_1=0.5). The diffractograms were recorded in the 2θ range of 2° - 90° with a step size of 0.04° and a scan time of 35 s per step.

Nitrogen adsorption-desorption isotherms were measured at -196 °C in an ASAP-2000 equipment (Micromeritics). Prior the adsorption measurements, the samples were degassed at 400 °C under vacuum overnight. Specific surface areas were calculated following the Brunauer-Emmett-Teller (BET) model. The *t*-plot method was used to estimate the microporosity of zeolites and catalysts. Total pore volumes were calculated at a relative pressure of 0.98. Pore size distributions were obtained following the Barret-Joyner-Halenda (BJH) methodology applied to the adsorption branch of the isotherms.

Metal dispersions were determined by H_2 chemisorption at 35 °C in a Quantachrome Autosorb-1C equipment using the double isotherm method, assuming an atomic H:M (M= Ir, Pt) adsorption stoichiometry of 1:1. Prior to adsorption, the samples were reduced in situ in flowing pure hydrogen at the same reduction conditions applied before catalysis (380 °C, 2 h).

The acidity of zeolites and calcined catalysts was studied by FTIR spectroscopy of adsorbed pyridine in a Nicolet 710 FTIR spectrometer. To this purpose, self-supported wafers (ca. 10 mg/cm^2) were prepared and degassed at 400 °C overnight under dynamic vacuum (10^{-6} mbar). Then, $1.8\cdot10^3$ Pa of pyridine were admitted to the IR cell and, after equilibration at room temperature (RT), the samples were degassed at 250 °C, the IR-pyridine spectrum recorded at RT, and the background spectrum subtracted. The concentrations of Brønsted and Lewis acid sites were obtained from the integrated areas of the IR pyridine bands at ca. 1450 and 1545 cm^{-1}, respectively, using the molar extinction coefficients reported by Emeis [29].

Transmission electron microscopy (TEM) was performed in a JEOL 2100F microscope operating at 200 kV to visually assess the generation of mesopores in zeolite beta upon the desilication treatment. Metal nanoparticles were characterized, prior reduction of catalysts in H_2 at 380 °C for 2 h, by scanning-transmission electron microscopy using a high-angle annular dark-field detector (HAADF-STEM) in the same microscope. Before observation, the solids were suspended in CH_2Cl_2, ultrasonicated for several minutes, and a solution drop deposited on a holey carbon-coated copper grid (300 mesh). The volume-area mean diameter of metal nanoparticles (d_{VA}) was calculated assuming spherical morphology upon measuring about 400 particles in micrographs taken at different positions on the grid, according to the equation $d_{VA} = \Sigma n_i\cdot d_i^3/\Sigma n_i\cdot d_i^2$, where n_i is the number of particles with diameter d_i. Then, the active metal surface area (AMSA, in m^2_{Me}/g_{cat}, Me= Ir, Pt) was estimated from d_{VA} values using the following formula [30]: $AMSA = (B/d_{VA})\cdot W_{Me}$, where B equals 2.68 and 2.80 for Ir and Pt, respectively, and W_{Me} stands for the metal loading (in wt%).

2.4. Catalytic experiments

The selective ring opening (SRO) of decalin (anhydrous ≥99%, Sigma-Aldrich, *cis/trans* molar ratio of ca. 50:50), commonly used as a model bi-naphthenic reactant, was carried out in a down-flow fixed bed reactor at total pressure of 3.5 MPa and weight hourly space velocity (WHSV, referred to decalin) of 0.44 h^{-1}. The reaction temperature was varied in the range of 220 to 275 °C to achieve decalin conversions ranging from ca. 10-20% up to above 95%. The SRO experiments were intentionally performed using a high H_2/decalin molar ratio of 100 to ensure a stable catalyst performance with time on stream, as shown in Figure S1 (Supporting Information) for the studied Ir(Pt)/Cs-β catalysts. In a typical experiment, the reactor was charged with 1.0 g of catalyst previously crushed and sieved to a pellet size of 0.25 - 0.42 mm and diluted with SiC granules (0.59-0.84 mm) to achieve a constant bed volume of 6.5 cm^3. Before

starting the reaction, the catalysts were reduced in situ at atmospheric pressure and 380 °C for 2 h (heating rate of 1 °C/min) under flowing pure hydrogen (200 cm^3/min). Preliminary experiments using the Ir/Cs-β-com catalyst were performed to ensure the absence of mass transfer restrictions at the investigated conditions (Figure S2).

Reaction products were regularly analyzed online by gas chromatography in a Brucker 450 GC equipped with a capillary column (BR-1 FS, 50 m x 0.25 mn x 0.5 µm) and a flame ionization detector (FID). The online GC analyses were used to determine the conversion of decalin (by grouping *cis*- and *trans*-decalin isomers) and the carbon-number distribution of reaction products. Due to the complex product mixture resulting from the conversion of decalin, with more than 200 peaks detected in the GC analyses, the reaction products were condensed after the online GC and the liquid fraction analyzed by comprehensive two-dimensional gas chromatography coupled to a mass spectrometry detector (GCxGC-MSD) to discriminate between similar hydrocarbon structures, as previously reported [31]. In particular, we used the GCxGC-MSD analyses to derive the relative amount of different types of C_{10} hydrocarbon products, namely decalin isomers (isoD), C_{10}-alkylcyclohexanes and C_{10}-alkylcyclopentanes (resulting from the opening of one C_6-ring of decalin, grouped here as ROP), and acyclic C_{10}-alkanes (iso-decanes + n-decane), commonly denoted as open chain decanes (OCD), formed upon opening of the remaining C_6-ring in ROP. The GCxGC-MSD analyses of condensed liquids were carried out in an Agilent 7890A gas chromatograph equipped with two detectors (MS Agilent 5977A detector and FID) and two columns (Column I: HP-INNOWAX of 30 m x 250 µm x 0.25 µm, and Column II: DB-5 of 5 m x 250 µm x 0.25 µm) connected in series through a flow modulator. A 2D view of a typical GCxGC chromatogram with the different C_{10} hydrocarbon classes identified is shown in Figure S3 (Supporting Information).

Decalin dehydrogenation products (tetralin, naphthalene) and hydrocarbons with more than 10 carbon atoms were not detected at the studied experimental conditions. On the other hand, the modified selectivity (S_j*, in mole %) of light (C_1 to C_9) hydrocarbons (grouped as C_{9-}) was used to derive information on the contribution of the β-scission (on zeolite Brønsted acid sites) and hydrogenolysis (on metal sites) mechanisms to the cleavage of C-C bonds, as proposed in earlier works [32-33]. The S_j* parameter, calculated according to Equation 1, is defined as the number of moles of hydrocarbons with *j* carbon atoms (n_j) formed divided by the amount of moles of decalin converted to C_{9-} products. According to this definition, the sum of S_j* for all cracked products (ΣS_j*, *j* = 1 - 9) can assume values ranging from 200%, indicative of a pure primary hydrocracking where only one C-C bond of the C_{10} hydrocarbon is cleaved, up to 1000% in the case all C-C bonds in C_{10} are cleaved producing 10 C_1 (methane) molecules.

$$S_j^* \text{ (mole \%)} = (n_{j\text{formed}}/n_{\text{decalin converted to C9-}}) \times 100 \qquad \text{Equation 1}$$

3. Results and discussion

3.1. Characterization of the materials

The chemical composition, textural properties, and acidity of pristine and alkali-exchanged zeolites and of corresponding Ir(Pt)/Cs-beta catalysts are given in Table 1. As expected, treatment of commercial beta zeolite with the basic CTAB+NaOH solution mixture decreased the bulk Si/Al atomic ratio from 18 to 16 as a result of partial desilication. After ionic exchange with Na^+ and then with Cs^+ cations, however, the Si/Al ratio of the mesoporous zeolite was restored to its original value of 18. This fact can be ascribed to the removal from the solid of most of the extraframework Al species formed during desilication under the slightly acidic pH of the exchanging Na^+/Cs^+ solutions (pH = 5.0 – 5.5), as supported by ^{27}Al MAS NMR characterization at different catalyst preparation stages (Figure S4). The Na content in the Cs-β-com and Cs-β-meso zeolites and corresponding catalysts was below 0.1 wt%, indicating that practically all Na^+ cations were replaced by Cs^+ during the second ionic exchange. Moreover, while incorporation of the metal function barely changed the Si/Al ratio of both Cs-beta samples, the Cs content in the final catalysts decreased notably (Table 1). This result hints at a partial exchange of Cs^+ cations by metal cations as well as by protons (H^+) upon contacting the Cs-zeolites with the slightly acidic solutions of the employed metal precursors (pH of 5.3 and 5.5 for the Ir and Pt solutions, respectively). Therefore, the ionic exchange with the alkali cations and the metal precursors are expected to modify the acid properties of the materials, as will be discussed later based on FTIR-pyridine measurements.

As shown in Table 1, the controlled desilication of β-com with NaOH in the presence of CTAB remarkably increased the mesopore area (S_{meso}) from 164 to 400 m^2/g at the expense of a relatively small loss (~ 25%) of zeolite microporosity, as inferred from the decrease in micropore volume (V_{micro}) from 0.20 to 0.15 cm^3/g. This is in line with previous reports, which showed that the use of organic pore-directing agents such as tetrapropylammonium (TPA^+) or cetyltrimethylammonium (CTA^+) cations along with NaOH in the preparation of hierarchical zeolites by desilication allowed to preserve, to a large degree, the properties of the parent zeolite [18, 34].

The N_2 adsorption-desorption isotherms and the BHJ pore size distributions for β-com and the desilicated β-meso sample are shown in Figure 1.

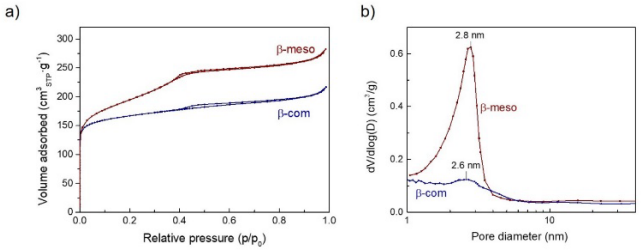

Figure 1. N_2 adsorption-desorption isotherms (a) and BHJ pore size distributions derived from the adsorption branch of the isotherms (b) for the original commercial beta (β-com) and the mesoporous beta (β-meso) samples.

As seen in Figure 1a, the commercial β-com sample exhibited a type I isotherm with a large increase in N_2 uptake at low relative pressures (< 0.1) and a limited uptake increase at higher relative pressures, corresponding to a mainly microporous material. In comparison to β-com, the desilicated β-meso sample showed an enhanced N_2 uptake, resulting in a higher BET area (756 m^2/g vs. 681 m^2/g, Table 1). Moreover, aside from the large uptake at low relative

pressures due to adsorption in micropores, the β-meso zeolite presented a sharp increase in N_2 uptake at a relative pressure of 0.3 – 0.4 (Figure 1a). This clearly signs for the presence of additional mesopores (besides those associated to the intercrystal space responsible for the increase in N_2 uptake at $p/p_0 > 0.95$ in both β-com and β-meso) in β-meso zeolite after the basic leaching process [10, 14, 18, 35]. The formation of mesopores induced by the alkaline CTAB+NaOH treatment is also evidenced by comparing the pore size distributions for β-com and β-meso samples in Figure 1b. As seen there, the mesopores generated in β-meso span a relatively narrow diameter range from about 2 to 4 nm with a maximum centered at around 2.8 nm. Similarly-sized mesopores (3 – 4 nm) have been reported for hierarchical beta zeolites prepared by desilication with NaOH in presence of CTA^+ cations [35].

Direct evidence for the development of mesoporosity upon desilication of the original β-com sample was gained from TEM observation, where the presence of intracrystalline mesopores was clearly evidenced in the alkaline-treated β-meso zeolite (Figure 2). Most of the formed mesopores ranged 2 – 4 nm in size (encircled regions in Figure 2b), in fair agreement with the value of around 3 nm derived from N_2 adsorption measurements (Figure 1b).

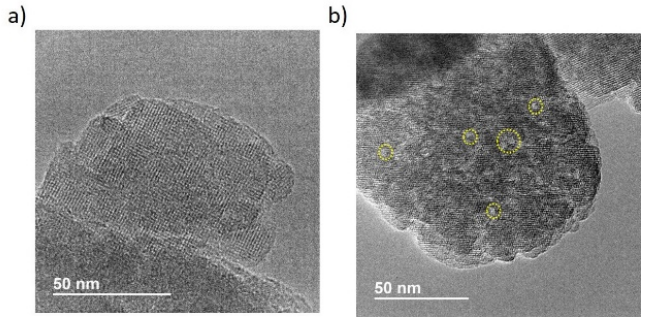

Figure 2. Representative TEM images for a) the commercial (β-com) and b) the alkaline-treated (β-meso) zeolites. Mesopores sizing ca. 2 – 4 nm formed in β-meso are encircled for better visualization.

The XRD patterns of the bare beta zeolites and corresponding Ir(Pt)/Cs-beta catalysts are presented in Figure 3. All samples exhibit the characteristic reflections of the BEA zeolite structure, with the most intense peaks located at around 7.5° and 22.5° (2θ). It can be seen in Figure 3 that the crystalline BEA structure was retained after the desilication treatment. For both beta samples, a decrease in the intensity of the BEA reflections after ionic exchange with Cs^+ is apparent in Figure 3, which can be attributed to scattering effects of the Cs^+ cations residing within the zeolite pores rather than to a real loss of crystallinity (i.e., partial amorphization) [33]. This is supported by the comparable micropore volumes of the initial beta zeolites and their respective Cs-exchanged samples (Table 1). Furthermore, the crystallinity of the calcined metal/Cs-beta catalysts remained similar to that of the respective Cs-exchanged zeolites (Figure 3).

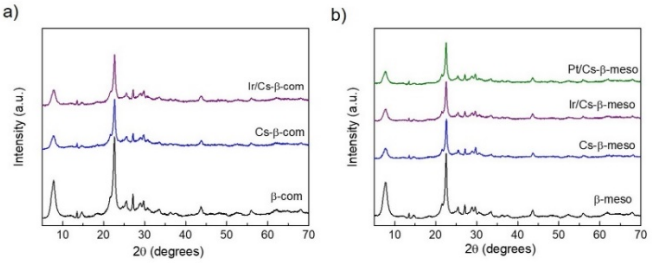

Figure 3. XRD patterns of zeolites and calcined metal/Cs-beta catalysts derived from the commercial (a) and mesoporous (b) beta samples.

The acid properties of the beta zeolites and the corresponding catalysts were assessed by IR spectroscopy. In the –OH stretching vibration region (Figure S3 of Supporting Information), both β-com and β-meso zeolites exhibited an intense IR band at 3745 cm^{-1} with a tail at ca. 3730 cm^{-1} that are assigned to silanol (Si-OH) groups on the external surface and in internal defects, respectively [36]. Moreover, a band at ca. 3609 cm^{-1} attributed to bridging Si-(OH)-Al groups associated to Brønsted acid sites [36] is also observed in both samples. As seen in Figure S5, the intensity of the 3745 cm^{-1} band of external silanols raised upon the desilication treatment due to the increased external surface area (S_{meso}, Table 1) related to the generation of additional mesopores. Concomitantly, β-meso showed a decreased intensity of the IR band at 3609 cm^{-1} in comparison to β-com, signing for some dealumination (and consequent loss of Brønsted acid sites) occurring during desilication, as supported by ^{27}Al MAS NMR spectroscopy (Figure S4).

FTIR spectroscopy of adsorbed pyridine was performed to estimate the density of Brønsted and Lewis acid sites in the beta zeolites and calcined Ir(Pt)/Cs-β catalysts.

Table 1. Chemical composition (ICP-OES), textural properties (N_2 adsorption), and acidity (FTIR-pyridine) of beta zeolite supports and Ir(Pt)/Cs-beta catalysts.

	ICP-OES		N_2 adsorption[a]			FTIR-pyridine[b]	
Sample	Si/Al ratio	Cs (wt%)	S_{BET} (m^2/g)	S_{meso} (m^2/g)	V_{micro} (cm^3/g)	BAS_{250} (μmol/g)	LAS_{250} (μmol/g)
β-com	18	-	681	164	0.20	248	60
Cs-β-com	18	7.9	627	164	0.18	3	26
Ir/Cs-β-com	18	5.0	590	157	0.17	73	110
β-meso	16	-	756	400	0.15	206	98
Cs-β-meso	18	8.2	725	370	0.15	2	26
Ir/Cs-β-meso	18	3.7	666	351	0.13	124	116
Pt/Cs-β-meso	18	3.1	664	365	0.14	117	102

[a] S_{BET} = BET surface area; S_{meso} = area of mesopores; V_{micro} = micropore volume.
[b] BAS_{250} and LAS_{250} are, respectively, the amounts of Brønsted and Lewis acid sites measured at a pyridine desorption temperature of 250 °C.

The FTIR-pyridine spectra at a pyridine desorption temperature of 250 °C are shown in Figure S6, and the quantitative results are gathered in Table 1. As observed, the alkaline treatment decreased the amount of Brønsted acid sites from 248 (β-com) to 206 (β-meso) μmol/g and concomitantly increased that of Lewis acid sites (from 60 to 98 μmol/g) due to partial dealumination and generation of extraframework Al species, as discussed before. As anticipated, the exchange of H^+ in the initial beta samples with Na^+ and then with Cs^+ cations drastically reduced the concentration of Brønsted acid sites to very low levels (2 – 3 μmol/g). Likewise, the amount of Lewis acid sites was also lowered from 60-98 to 26 μmol/g, which can be related to the removal of most of the extraframework Al species present in the original zeolites during the exchange with alkali cations (Figure S4). As seen in Table 1, the incorporation of the metal function via ionic exchange remarkably raised the amount of Brønsted acid sites from 2-3 to 73-124 μmol/g as the result of the exchange back of some Cs^+ cations by H^+. The higher density of Brønsted acid sites of Ir(Pt)/Cs-β-meso (117 – 124 μmol/g) samples relative to Ir/Cs-β-com (73 μmol/g) can be bridged to the higher extent of exchange of Cs^+ by H^+ in the former, as concluded from their lower Cs contents (Table 1).

The metal content in the Ir(Pt)/Cs-β catalysts estimated by FESEM-EDX ranged from 3.1 to 3.5 wt% (Table 2), slightly exceeding the nominal value of 3 wt%. On the other hand, the metal dispersion after reduction of catalysts in flowing H_2 at 380 °C for 2 h was assessed by H_2 chemisorption and electron microscopy (TEM and HAADF-STEM).

Table 2. Properties of the metal species in the H_2-reduced Ir(Pt)/Cs-β catalysts determined by H_2 chemisorption and electron microscopy (STEM).

Catalyst	Metal content[a] (wt%)	D_{Me}[b] (%)	Mean metal particle size[c] (nm)		AMSA[d] (m^2/g_{cat})
			d_{H2}	d_{VA}	
Ir/Cs-β-com	3.2	140	0.7	1.3	6.6
Ir/Cs-β-meso	3.4	120	0.8	1.7	5.4
Pt/Cs-β-meso	3.5	80	1.4	1.6	5.6

[a] Determined by FESEM-EDX.
[b] From H_2 chemisorption measurements.
[c] d_{H2} = Mean metal particle size estimated by H_2 chemisorption; d_{VA} = volume-area mean diameter of metal particles determined by STEM.
[d] Active metal surface area (see Experimental).

Extremely high metal dispersions (120% – 140%) were obtained from H_2 chemisorption data for the Ir-based catalysts regardless the porosity of the starting Cs-β sample (Table 2). Ir dispersions above 100% have been associated with an adsorption stoichiometry H:Ir above 1:1 [6, 33]. According to the earlier literature, H:Ir adsorption stoichiometry ratios above 1:1 are likely attributed to multiple bonding of H atoms occurrring on coordinatively unsaturated Ir atoms (e.g., in corners and steps) abundantly present in very small metal crystallites [37-38]. The chemisorption-derived dispersions translated into mean metal particle sizes (d_{H2}, Table 2) of ca. 0.7 – 0.8 nm. As for Pt, for which an adsorption stoichiometry H:Pt = 1:1 is commonly assumed [39-40], a somewhat lower (but still high) dispersion of 80% (corresponding to a mean Pt particle size of 1.4 nm) was obtained in comparison to the equivalent Ir-containing catalyst (Table 2).

The metal particle size for the H_2-reduced catalysts was also analyzed by HAADF-STEM. Representative STEM images and derived metal particle size distributions are shown in Figure 4. As observed, small-sized (ranging 0.5 – 2.5 nm) metal nanoparticles, appearing as bright spots in the HAADF-STEM images, were apparent for all catalysts, in good agreement with the very high dispersions inferred from H_2 chemisorption. In fact, all catalysts displayed alike volume-area mean metal particle sizes of 1.3 – 1.7 nm (d_{VA}, Table 2). It is worth noting that, while for the Ir-based catalysts the d_{VA} values (1.3 – 1.7 nm) were higher than the mean particle sizes estimated from H_2 chemisorption (0.7 – 0.8 nm) due to the uncertainty in the H:Ir adsorption stoichiometry, a good correspondence between both techniques was observed for the Pt/Cs-β-meso catalyst (1.4 vs. 1.6 nm, Table 2).

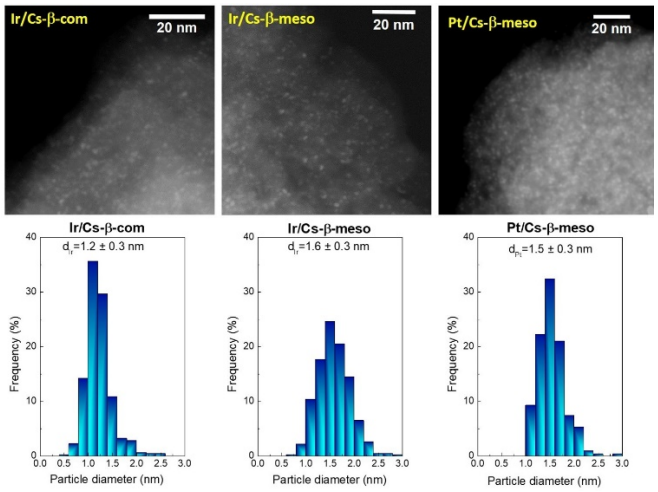

Figure 4. Representative HAADF-STEM micrographs and corresponding metal particle size histograms (shown at the bottom of each image) for the Ir(Pt)/Cs-β catalysts.

As seen in Table 2, the Ir catalyst based on the commercial zeolite displayed a somewhat lower mean particle size (1.3 nm) compared to that based on the mesoporous sample (1.7 nm), translating into a slightly higher active metal surface area (AMSA) of the former (6.6 m^2/g_{cat} for Ir/Cs-β-com vs. 5.4 m^2/g_{cat} for Ir/Cs-β-meso). However, a similar mean particle size (1.6 – 1.7 nm) resulting in an alike AMSA

value (5.4 – 5.6 m^2/g_{cat}) was obtained for the Ir and Pt catalysts dispersed on Cs-β-meso.

In summary, both H_2 chemisorption and electron microscopy signed for a very high metal dispersion in the prepared Ir(Pt)/Cs-β catalysts, a feature that is highly relevant to promote the opening of naphthenic rings through the selective hydrogenolysis mechanism, as will be discussed next.

3.2. SRO of decalin on Ir(Pt)/Cs-β catalysts

Even if a nearly equimolar mixture of *cis*- and *trans*-decalin was fed to the reactor (*trans*-D/(*cis*-D+*trans*-D) ~ 0.5), the *trans*-D/(*cis*-D+*trans*-D) ratio in the product stream raised to ca. 0.94 – 0.88 for all catalysts in the studied temperature range (220 – 275 °C). These values match well the predicted thermodynamic ratios (0.94 – 0.89) at similar temperatures (250 – 380 °C) [33], indicating that a rapid *cis*-to-*trans* stereoisomerization to the equilibrium mixture occurred over the Ir(Pt)/Cs-β catalysts, in agreement with what has been reported for analogous Ir- and Pt-zeolite systems [6, 32-33, 41-42]. Therefore, in the following both *cis*- and *trans*-decalin are grouped and considered as a single reactant molecule (decalin) for calculating conversions and product yields/selectivities. It has been suggested that, over bifunctional Pt(Pd)/H-zeolite catalysts, the *cis*-to-*trans* stereoisomerization of decalin may take place both via dehydrogenation-hydrogenation reactions involving olefinic (i.e., octalin) intermediates on the metal [43] and via carbocations on the zeolite acid sites [33, 41].

3.2.1. Catalyst activity. The conversion of decalin over the bifunctional Ir(Pt)/Cs-β catalysts is depicted in Figure 5 as a function of reaction temperature. Among the Ir catalysts, that based on the mesoporous beta zeolite (Ir/Cs-β-meso) displayed, at a given reaction temperature, a higher decalin conversion compared to its homologous catalyst based on the commercial zeolite (Ir/Cs-β-com). In principle, this could be ascribed to the higher density of Brønsted acid sites of Ir/Cs-β-meso (Table 1) and their role in promoting the isomerization of C_6 to C_5 naphthenic rings (i.e., ring contraction), thus facilitating the subsequent ring opening of the formed iso-decalin products (isoD) on the metal sites, as concluded in previous studies using bifunctional Ir(Pt)-zeolite catalysts [4, 6, 41]. However, as will be shown in the next section, the fact that the yield of isoD on both Ir/Cs-β catalysts was very low (< 1 wt%) in the whole range of decalin conversions makes unlikely an enhanced formation of isoD on Brønsted acid sites (via bifunctional catalysis) as the origin of the higher activity of Ir/Cs-β-meso vs. Ir/Cs-β-com. Moreover, the activity trend observed for the Ir catalysts can neither be explained considering the amount of active metal sites on which C-C bond cleavage may occur via hydrogenolysis, since the less active Ir/Cs-β-com exhibited a slightly lower metal particle size and, consequently, a somewhat larger active metal surface area than Ir/Cs-β-meso (Table 2). Therefore, we attribute the higher activity of Ir/Cs-β-meso for decalin conversion to an enhanced accessibility of active metal sites induced by the presence of the intra-crystal mesopores generated during the controlled desilication treatment.

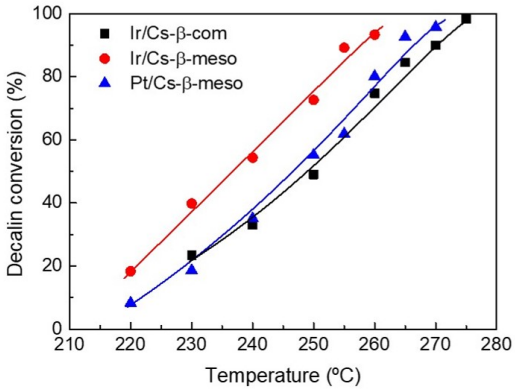

Figure 5. Conversion of decalin as a function of reaction temperature for the Ir(Pt)/Cs-β catalysts. Reaction conditions: P = 3.5 MPa, WHSV = 0.44 h^{-1}, H_2/decalin = 100 mol/mol.

The influence of the nature of the hydrogenolysis metal (Ir vs. Pt) dispersed on the mesoporous Cs-β-meso zeolite was also investigated. Both Ir/Cs-β-meso and Pt/Cs-β-meso possessed alike porosity and density of Brønsted acid sites (~ 120 μmol/g, Table 1) as well as similar mean metal particle size (and active metal surface area) after reduction in H_2 as measured by electron microscopy (1.6 – 1.7 nm, Table 2). It can be seen in Figure 5 that the Ir catalyst is more active than the Pt one, requiring lower temperatures (by ca. 10 °C) to achieve a given decalin conversion. This trend reflects the well known higher hydrogenolysis activity of Ir to break endocyclic unsubstituted C-C bonds, as those present in the C_6 naphthenic decalin rings, through the dicarbene mechanism [3]. At variance with the behaviour observed for Ir, a certain amount of decalin skeletal isomers (isoD), containing at least one C_5 ring and thus more prone to undergo ring opening on metal sites compared to decalin, were formed on the Pt catalyst (see next section). Therefore, at comparable metal dispersion (particle size), Ir is more active than Pt for converting decalin in spite of a higher formation of isoD products in the later catalyst.

3.2.2. Overall product yields and selectivities. The yield of the different product groups for the Ir(Pt)/Cs-beta catalysts is shown in Figure 6 as a function of decalin conversion. At low-to-moderate conversions (20 – 40%), ROP followed by OCD were the main products formed on the Ir catalysts while only minor amounts of isoD (yield < 1 wt%) were observed in the whole conversion range, as mentioned before. For these catalysts, the yield of ROP and OCD increased with decalin conversion, reached a maximum at conversions of ca. 80 – 90%, and then declined at higher conversions coinciding with a nearly exponential increase in the yield of lighter (C_{9-}) hydrocarbons. The prevalence of ROP and the low yield of isoD at low-to-moderate decalin conversions observed for both Ir/Cs-β-com and Ir/Cs-β-meso catalysts resemble the behavior observed for Ir-containing HIPEROC systems based on K^+- or Cs^+-exchanged FAU or BEA zeolites [6, 33], as anticipated from their common features of i) relatively high metal loading (3.0 – 3.5 wt% Ir), ii) high metal dispersion, and iii) low density of Brønsted acid sites. The Brønsted acidity in HIPEROCs is kept low in order to promote the formation of decalin skeletal isomers (isoD) while preventing extensive cracking,

whereas ring opening of C_5 naphthenic rings in the formed isoD occurs predominantly via hydrogenolysis on the metal. On such catalysts, a certain contribution of the "direct ring opening" pathway, characteristic of Ir/SiO_2 [44] and Ir/Al_2O_3 [45] catalysts lacking Brønsted acid sites, to the overall decalin conversion was shown to occur. It is worth noting that, even at relatively low decalin conversions (20 – 25%), the selectivity of isoD is notably lower and that of ROP higher in our Ir/Cs-β catalysts compared to the most efficient HIPEROCs based on beta zeolite (catalyst 3.4Ir/H,Cs-Beta in ref. [6]) (see Figure S7 in Supporting Information). This may sign for a greater contribution of the "direct ring opening" route relative to the bifunctional pathway in the Ir/Cs-β catalysts studied in the present work due, most probably, to the higher Ir dispersion (hence, exposing, at comparable Ir contents, a greater metallic surface area) achieved in our Ir/Cs-β catalysts (120 – 140% according to H_2 chemisorption, Table 2) relative to that reported for 3.4Ir/H,Cs-Beta (86%) [6].

The most salient feature of the mesoporous Ir/Cs-β-meso catalyst is, as seen in Figure 6, its remarkably higher yield of desired OCD and lower yield of C_{9-} hydrocarbons compared with Ir/Cs-β-com, especially at conversions above 50%. Moreover, the conversion at which the maximum yields of ROP and OCD are attained is shifted to higher values (~ 90%) in Ir/Cs-β-meso with respect to Ir/Cs-β-com (~ 80 – 85%). These features suggest an enhanced diffusion of ROP and OCD products in the mesoporous catalyst retarding their further conversion into ligther compounds, and highlight the benefit of introducing additional mesopores in the commercial beta zeolite

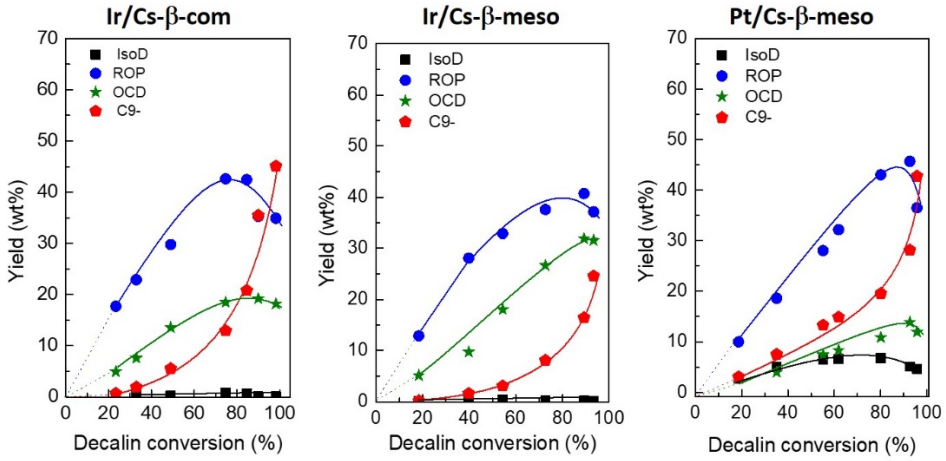

Figure 6. Yields of the different product fractions as a function of decalin conversion for the Ir(Pt)/Cs-β catalysts. Reaction conditions: T = 220 – 275 °C, P = 3.5 MPa, WHSV = 0.44 h^{-1}, H_2/decalin = 100 mol/mol.

through controlled desilication for improving the yield of target ring opening products. In fact, as shown in Table 3, the Ir catalyst based on the mesoporous zeolite exhibits the highest maximum yield of OCD (31.9 wt%) and combined yield of ROP+OCD (72.6 wt%) while concomitantly yielding the lowest amount of unwanted C_{9-} hydrocarbons (16.4 wt%). The value for the maximum combined yield of ROP+OCD achieved over Ir/Cs-β-meso (72.6 wt%) is the highest ever reported in the SRO of decalin over zeolite-supported Ir or Pt catalysts, including the best-performing HIPEROC systems, although with a somewhat lower maximum yield of target OCD (Table S1). Nonetheless, the maximum yield of OCD attained over Ir/Cs-β-meso (32 wt%) exceeds the criterium of a minimum yield of 25% (starting from decalin) established for a selective ring opening catalyst to be considered HIPEROC [6].

On the other hand, the catalyst comprising Pt dispersed on the mesoporous beta zeolite (Pt/Cs-β-meso) showed a somewhat different yield-conversion behaviour in comparison to the Ir-based catalysts. While, similarly to the Ir-based catalysts, ROP were the main products formed on Pt/Cs-β-meso, the yields of isoD and C_{9-} were enhanced and that of OCD lowered in the Pt catalyst compared to the Ir ones (Figure 6). Main isoD products found by GCxGC-MSD on Pt/Cs-β-meso were spiro[4.5]decane, methylbicyclo[4.3.0]nonanes, methylbicyclo[3.3.1]nonanes, and dimethylbicyclo[3.2.1]octanes (Figure S8a). The yield of these isoD products is shown in Figure S8b as a function of decalin conversion. At low conversions (X_{dec} ~ 20%), spiro[4.5]decane is the prevailing decalin isomer with a clear primary character. The yield of spiro[4.5]decane gradually decreases at increasing conversions while the yield of methylbicyclo[4.3.0]nonanes and methylbicyclo[3.3.1]nonanes first increases, reaches a maximum at conversions of ca. 60 – 70%, and then drops at higher conversions. In turn, dimethylbicyclo[3.2.1]octanes start to be observed at conversions above 20%, indicative of their secondary nature. Their yield increases with conversion until a maximum is reached at a conversion of ca. 90%, above which it starts to decline. This yield-conversion trend is consistent with dimethylbicyclo[3.2.1]octanes being formed by branching isomerization of methylbicyclononanes. While methylbicyclononanes and dimethylbicyclooctanes are unambiguously formed by acid-catalyzed skeletal isomerization of decalin through the classical bifunctional mechanism [41], the formation of spiro[4.5]decane as a primary product can be accounted for both by the bifunctional pathway [33] and by a metal-catalyzed mechanism on Pt sites as it has been reported for monofunctional Pt/SiO_2 catalysts [44].

Table 3. Product yields attained over Ir(Pt)/Cs-β catalysts at the condition of maximum yield of high cetane OCD products ($Y_{OCD,max}$). Reaction conditions: P = 3.5 MPa, WHSV = 0.44 h^{-1}, H_2/decalin = 100 mol/mol.

Catalyst	T (°C)	X_{Dec} (%)	Y_{ROP} (wt%)	$Y_{OCD,max}$ (wt%)	$Y_{ROP+OCD,max}$ (wt%	Y_{C9-} (wt%)
Ir/Cs-β-com	265	84.6	42.4	20.7	63.1	20.8
Ir/Cs-β-meso	255	89.2	40.7	**31.9**	**72.6**	16.4
Pt/Cs-β-meso	265	92.7	45.7	13.9	59.6	28.1

The selectivity-conversion curves for the Ir(Pt)/Cs-β catalysts are presented in Figure S9a of Supporting Information. As inferred from the isoD yields shown in Figure 6, both Ir/Cs-β-com and Ir/Cs-β-meso catalysts exhibit a very low selectivity to isoD in the whole conversion range. On these catalysts, ROP appear as primary unstable products whereas OCD exhibit a clear secondary unstable behaviour. Moreover, the negligible selectivity of C_{9-} products at low decalin conversions and its progressive raise at increasing conversions sign for their secondary and stable character. These selectivity trends are in concordance with the general reaction scheme shown in Figure S9b, according to which ROP are predominantly formed by direct ring opening of decalin, OCD are produced by opening the remaining naphthenic ring in ROP, and light (C_{9-}) hydrocarbons are formed from both ROP and OCD. A somewhat different selectivity pattern is observed for the Pt/Cs-β-meso catalyst (Figure S9a). In this case, both isoD and ROP appear as primary products with selectivities of ca. 20 and 60 wt%, respectively, at around 20% conversion. However, the slope in the lower conversion range (< 40%) of the ROP selectivity curve for Pt/Cs-β-meso is notably smaller than that for the Ir-based catalysts, which suggests that ROP in the former are likely formed from both decalin (direct ring opening) and isoD, as discussed previously. Similarly to the Ir/Cs-β samples, OCD and C_{9-} hydrocarbons show, respectively, a secondary-unstable and secondary-stable character, according to the general reaction scheme presented in Figure 9b for Pt/Cs-β-meso.

3.2.3. Internal distribution of ROP. The composition of the ROP fraction derived from GCxGC-MSD analyses is presented in Figure 7 for the studied Ir(Pt)/Cs-β catalysts at low-to-moderate decalin conversions (X_{dec} = 30 – 40%). At these conditions, major ROP compounds obtained for the two Ir-based catalysts were 1-methyl-2-propylcyclohexane and 1,2-diethylcyclohexane, representing about 54 – 61% and 21 – 30%, respectively, of the total ROP fraction. The prevalence of these two ROP isomers at low conversions, as also found for monofunctional (non-acidic) Ir/SiO_2 [44] and Ir/Al_2O_3 [45] as well as for bifunctional Ir/zeolite HIPEROC-type catalysts [6], and their presence in a 1-methyl-2-propylcyclohexane/1,2-diethylcyclohexane ratio close to 2:1 clearly indicate that they originate from the direct ring opening of decalin by cleavage at unsubstituted (secondary – secondary) C-C bonds on iridium via dicarbene intermediates [45]. The absence of butylcyclohexane (Figure 7) is also consistent with ring opening occurring preferentially via the dicarbene mechanism on the Ir/Cs-β catalysts [33, 44]. Besides the direct ring opening products, the most abundant ROP isomers formed on Ir/Cs-β were ethyldimethylcyclohexanes, accounting for ca. 8 – 21% of all ROP, which are typically formed by ring opening of skeletal decalin isomers via acid catalysis [2, 45]. As evidenced in Figure 7, the relative amount of 1-methyl-2-propylcyclohexane + 1,2-diethylcyclohexane within ROP is notably higher for Ir/Cs-β-meso (91%) in comparison with Ir/Cs-β-com (74%), suggesting a greater contribution of the metal-catalyzed direct ring opening pathway in the mesoporous catalyst, in agreement with its higher activity, as discussed previously (Figure 5).

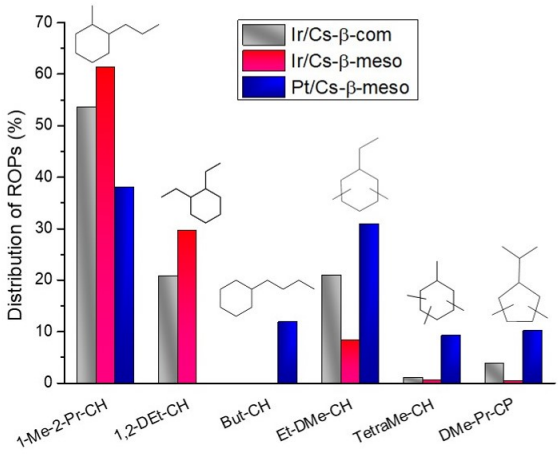

Figure 7. Distribution of main ROP isomers obtained the Ir(Pt)/Cs-β catalysts at a decalin conversion of 30 – 40%. Abbreviations: 1-Me-2-Pr-CH = 1-methyl-2-propylcyclohexane; 1,2-DEt-CH = 1,2-diethylcyclohexane; But-CH = butylcyclohexane; Et-DMe-CH = ethyldimethylcyclohexanes; TetraMe-CH = tetramethylcyclohexane; DMe-Pr-CP = dimethylpropylcyclopentanes.

Differently from the Ir catalysts, butylcyclohexane (representing about 12% of all ROP at 30 – 40% conversion, Figure 7) was observed in the Pt-based mesoporous sample. This ROP isomer normally originates from the direct ring opening of a secondary – tertiary C-C bond of decalin on Pt centers according to the multiplet (e.g., non-selective) mechanism [44]. Moreover, compared to Ir, higher amounts of ethyldimethylcyclohexanes, dimethylpropylcyclopentanes (predominantly dimethylisopropylcyclopentane), and tetramethylcyclohexane, all typically produced by β-scission of endocyclic C-C bonds of skeletal decalin isomers on Brønsted acid sites [45,41], were obtained on the Pt catalyst. This results in a remarkably lower relative contribution of direct ring opening products to total ROP for the mesoporous Pt catalyst (ca. 50%) compared with its Ir counterpart (91%), concurring with the trends reported in the SRO of decalin over zeolite Y-based Pt and Ir catalysts [33].

3.2.4. Internal distribution of OCD. Opening of the remaining napthenic ring in ROP leads to the formation of open chain alkanes (e.g., C_{10} alkanes), the most desirable ring opening products from the cetane viewpoint [2]. As shown in Figure 8, a similar distribution of OCD was observed for the two Ir-based catalysts, with dimethyloctanes as the most abundant isomers contributing by about 60% (for Ir/Cs-β-com) and 67% (for Ir/Cs-β-meso) to the total OCD at 30 – 40% decalin conversion. The second major OCD isomers were monobranched

isodecanes (methylnonanes + 4-ethyloctane, constituting about 27 – 30% of all OCD), followed by trimethylheptanes (5 – 10%). Therefore, about 70% of OCD formed on Ir/Cs-β were multibranched isomers, a value that is comparable to that reported for Ir/SiO_2 lacking Brønsted acid sites [44]. Moreover, no n-decane was observed for any of the two Ir-based catalysts. The relatively high proportion of multibranched decanes along with the absence of n-decane is in conformity with OCD being formed predominantly by hydrogenolysis of endocyclic unsubstituted C-C bonds on the metal sites of our Ir/Cs-β catalysts according to the dicarbene mechanism. Overall, these results show that the generation of additional mesopores in zeolite beta by desilication has a minor influence on the molecular structure of the formed OCD products.

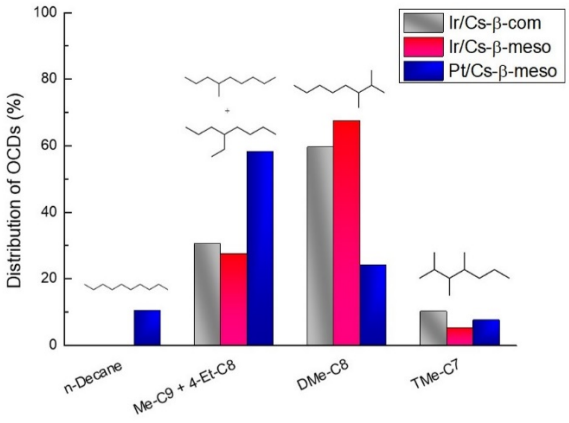

Figure 8. Distribution of OCD (open chain decanes) obtained the Ir(Pt)/Cs-β catalysts at a decalin conversion of 30 – 40%.

A significantly different distribution of OCD was obtained for the mesoporous Pt catalyst. In this case, contrary to Ir, n-decane was observed in the reaction products, constituting about 10% of all OCD at a decalin conversion of 30 – 40%. In addition, the predominant OCD compounds over the Pt catalyst were by far monobranched isomers (about 60% of the total OCD fraction), among which methylnonanes accounted for ca. 90% of all monobranched decanes. Overall, n-decane and monobranched isodecanes, exhibiting higher cetane numbers than multiply branched decanes [2], represented ca. 70% of all OCD formed on Pt/Cs-β-meso, in contrast to the 30% obtained for the Ir/Cs-β catalysts. The prevalence of less branched decanes in the Pt catalyst stems from the known preferential cleavage of endocyclic C-C bonds at substituted positions of ROP rings through the multiplet mechanism. Although in lower amounts, the presence of di- and tri-branched decanes, however, signs for a certain contribution of the bifunctional pathway involving carbocationic intermediates to the ring opening of ROP.

3.2.5. Selectivity pattern for C_{9-} hydrocarbons. Relevant information on the prevailing C-C bond cleavage mechanism (i.e., hydrogenolysis on metal sites vs. bifunctional on metal + Brønsted acid sites) leading to both ring opening products and lighter hydrocarbons can be gathered by analyzing the C_{9-} fraction through the so-called modified hydrocracking selectivity (S_j*), originally defined by Rabl et al. as the molar amount of product with *j* carbon atoms (*j* = 1 – 9) formed divided by the molar amount of decalin converted to C_{9-} hydrocarbons [32]. The modified hydrocracking selectivity, S_j*, for the studied Ir(Pt)/Cs-β catalysts at the condition of maximum combined yield of ROP+OCD is presented in Figure 9 as a function of the number of carbon atoms. Regardless of the zeolite porosity, the two Ir-based catalysts display a hammock-shaped S_j* curve, with high selectivity values for C_1 and C_9 and a nearly flat region of lower selectivity to C_3-C_7 hydrocarbons. This selectivity pattern is indicative for hydrogenolysis on Ir sites as the prevailing C-C bond cleavage mechanism in the Ir catalysts. Differently, the Pt-based catalyst shows an M-shaped S_j* pattern characterized by much lower selectivities to C_1 and C_9 and two pronounced maxima at C_4 and C_6 comprised mainly of isobutane (~ 60% of all C_4) and methylcyclopentane (~ 35% of all C_6), respectively, formed through the acid-catalyzed paring reaction [32]. This behavior reflects the prevalence of the hydrocracking mechanism to the cleavage of C-C bonds, via carbocations, in Pt/Cs-β-meso. The notably larger contribution of the bifunctional mechanism to the formation of ring opening and C_{9-} products in Pt/Cs-β-meso compared to the Ir-containing catalysts is in line with the enhanced formation of decalin skeletal isomers (isoD) in the former, as discussed previously (Figure 6).

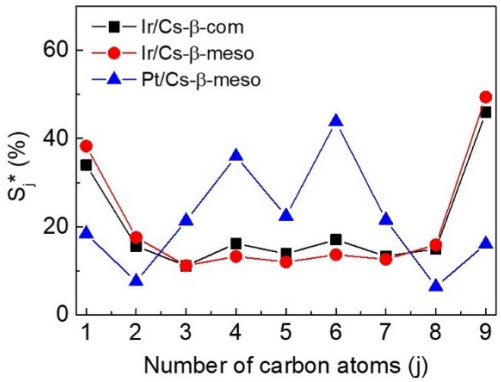

Figure 9. Modified hydrocracking selectivity (S_j*) as a function of the number of carbon atoms of C_1 – C_9 hydrocarbons in the conversion of decalin on Ir(Pt)/Cs-β catalysts at the conditions of maximum combined yield of ROP+OCD: T = 255 – 265 °C, P = 3.5 MPa, WHSV = 0.44 h^{-1}, H_2/decalin = 100 mol/mol.

Finally, it is worth mentioning that, at the studied conditions, the total modified hydrocracking selectivity (ΣS_j*, *j* = 1 – 9) for all three Ir(Pt)/Cs-beta catalysts reached values close to 200%, indicative of a nearly pure primary hydrocracking behaviour where only one C-C bond in a C_{10} hydrocarbon is cleaved leading to equimolar amounts of two lighter products.

4. Conclusions

Ir- and Pt-containing catalysts highly dispersed on low acidic mesoporous beta zeolite have been prepared and evaluated in the selective ring opening (SRO) of decalin as model naphthenic reactant. The mesoporous beta zeolite (β-meso) was produced by post-synthesis desilication of a commercial beta sample (β-com, Si/Al = 18) with NaOH in presence of cetyltrimethylammonium (CTA^+) cationic surfactant. Removal of the surfactant template by

calcination at 550 °C generated intra-crystal mesopores sizing 2 – 4 nm, as assessed by N_2 adsorption and TEM measurements, thereby increasing the mesopore area from 164 to 400 m^2/g while largely retaining the microporosity and acidity of the parent beta zeolite. Prior introduction of the metal function (either Ir or Pt in concentrations of ca. 3 – 3.5 wt%), the calcined β-meso zeolite was ionic exchanged with Na^+ and then with Cs^+ cations in order to minimize the contribution of unselective cleavage of C-C bonds via carbocations on Brønsted acid sites. According to H_2 chemisorption, a high metal dispersion (> 100% for Ir and 80% for Pt) was achieved upon deposition of the metal on the Cs-exchanged β-meso zeolite (Cs-β-meso) via ionic exchange with suitable metal precursors and subsequent calcination at 300 °C under high air space velocity (1 $L/(g_{cat}{\cdot}min)$) and slow ramping (0.2 °C/min). Such high metal dispersions were confirmed by HAADF-STEM, from which mean Ir and Pt particle sizes of 1.6 – 1.7 nm were derived. For comparative purposes, an Ir catalyst (3.2 wt% Ir) based on the parent commercial β-com sample was also prepared under the same conditions used for the mesoporous zeolite. In spite of their alike metal concentration and dispersion, the Ir catalyst based on mesoporous beta (Ir/Cs-β-meso) displayed higher decalin conversions at constant reaction conditions and achieved a higher maximum yield of ring opening products than that based on the original beta zeolite (Ir/Cs-β-com) due to an enhanced accessibility of the active sites in the former. Moreover, the additional mesopores produced in β-meso facilitated the transport rate of ring opening products (C_{10}-alkylcycloalkanes, ROP, and C_{10}-alkanes or open chain decanes, OCD) retarding their further conversion to unwanted lighter (C_{9-}) hydrocarbons. As a result, the Ir/Cs-β-meso catalyst achieved an outstanding maximum combined yield of ROP+OCD of 72.6 wt% at a decalin conversion of 89.2% (81.4% selectivity), which is the highest yield so far reported in the SRO of decalin. Comparatively, the Ir/Cs-β-com counterpart attained a maximum combined yield of ROP+OCD of 63.1 wt% at 84.6% conversion (74.6% selectivity). Furthermore, the maximum yield of OCD, the most desirable SRO products from the cetane viewpoint, reached 34.1 wt% over Ir/Cs-β-meso and only 20.7 wt% over Ir/Cs-β-com, further highlighting the beneficial role of the generated mesopores in minimizing undesired secondary reactions. For both Ir-based catalysts, the very low yields (< 1 wt%) of skeletal decalin isomers (isoD), the molecular structure of the main ROP and OCD isomers, assessed by comprehensive two-dimensional gas chromatography (GCxGC), and the hammock-type distribution of C_{9-} products are consistent with cleavage of C-C bonds occurring primarily on Ir sites through the (unselective) dicarbene mechanism.

In comparison to its Ir counterpart, the Pt catalyst dispersed on mesoporous beta (Pt/Cs-β-meso) was less active and attained both a lower maximum yield of ROP+OCD (59.6 wt%) and of OCD (13.9 wt%) at 92.7% conversion. However, compared to the Ir catalysts, Pt/Cs-β-meso produced less branched ROP and OCD products (i.e., with higher cetane), as expected from the (selective) multiplet hydrogenolysis mechanism prevailing on Pt sites that favors cleavage at substituted endocyclic C-C bonds. Moreover, the higher isoD yields and the M-shaped carbon number distribution of C_{9-} hydrocarbons sign for a significant contribution of the bifunctional pathway via carbocations, besides the metal-catalyzed hydrogenolysis route, to the cleavage of C-C bonds over Pt/Cs-β-meso.

To conclude, it may be anticipated that the benefits of using a properly designed SRO catalyst based on hierarchical (mesoporous) beta zeolite would be even more pronounced when treating bulkier naphthenes more representative of those present in real feeds.

Conflicts of interest

There are no conflicts to declare.

Acknowledgments

M.A. Arribas and A. Martínez acknowledge the MINECO of Spain for financial support through the Severo Ochoa project (SEV2016-0683). N. Suárez and A. Moreno acknowledge Colciencias-Ecopetrol (project 1115-559-36523) and Universidad de Antioquia (Colombia) for financial support. N. Suárez acknowledges Colciencia-Ecopetrol and the Instituto de Tecnología Química (ITQ). The authors are indebted to the Microscopy Service of the Universitat Politècnica de València for its assistance in microscopy characterization.

References

1. M.A. Arribas, A. Martínez, *Appl. Catal. A*, 2002, **230**, 203-217.
2. R. C. Santana, P.T. Do, M. Santikunaporn, W.E. Alvarez, J.D. Taylor, E.L. Sughrue, D.E. Resasco, *Fuel*, 2006, **85**, 643-656.
3. G. B. McVicker, M. Daage, M.S. Touvelle, C.W. Hudson, D.P. Klein, W.C. Baird, B.R. Cook, J.G. Chen, S. Hantzer, D.E.W. Vaughan, E.S. Ellis, O.C. Feeley, *J. Catal.*, 2002, **210**, 137-148.
4. A. Martínez, M.A. Arribas, S.B.C. Pergher, *Catal. Sci. & Technol.*, 2016, **6**, 2528-2542.
5. D. Kubička, N. Kumar, P. Mäki-Arvela, M. Tiitta, V. Niemi, T. Salmi, D.Y. Murzin, *J. Catal.*, 2004, **222**, 65-79.
6. D. Santi, T. Holl, V. Calemma, J. Weitkamp, *Appl. Catal. A*, 2013, **455**, 46-57.
7. M.A. Arribas, A. Martínez, G. Sastre, *Stud. Surf. Sci. Catal.*, 2002, **142**, 1015-1022.
8. M.A. Arribas, A. Corma, M.J. Díaz-Cabañas, A. Martínez, *Appl. Catal. A*, 2004, **273**, 277-286.
9. K. C. Mouli, V. Sundaramurthy, A.K. Dalai, Z. Ring, *Appl. Catal. A*, 2007, **321**, 17-26.
10. J. C. Groen, L.A.A. Peffer, J.A. Moulijn, J. Pérez-Ramírez, *Micropor. Mesopor. Mater.*, 2004, **69**, 29-34.
11. D. Verboekend, J. Pérez-Ramírez, *Catal. Sci. & Technol.*, 2011, **1**, 879-890.
12. D.P. Serrano, J.M. Escola, P. Pizarro, P., *Chem. Soc. Rev.*, 2013, **42**, 4004-4035.
13. J. Pérez-Ramírez, C.H. Christensen, K. Egeblad, C.H. Christensen, J.C. Groen, *Chem. Soc. Rev.*, 2008, **37**, 2530-2542.
14. J.C. Groen, S. Abelló, L.A. Villaescusa, J. Pérez-Ramírez, *Micropor. Mesopor. Mater.*, 2008, **114**, 93-102.
15. K. Zhang, M.L. Ostraat, *Catal. Today*, 2016, **264**, 3-15.
16. M.S. Holm, M.K. Hansen, C.H. Christensen, C. H., *Eur. J. Inorg. Chem.*, 2009, **2009**, 1194-1198.
17. J. García-Martínez, M. Johnson, J. Valla, K. Li, J.Y. Ying, *Catal. Sci. & Technol.*, 2012, **2**, 987-994.
18. D. Verboekend, G. Vilé, J. Pérez-Ramírez, *Cryst. Growth Des.*, 2012, **12**, 3123-3132.
19. N. Suárez, J. Pérez-Pariente, F. Mondragón, A. Moreno, *Micropor. Mesopor. Mater.*, 2019, **280**, 144-150.
20. Y. Yan, X. Guo, Y. Zhang, Y. Tang, *Catal. Sci. & Technol.*, 2015, **5**, 772-785.
21. K. Li, J. Valla, J. García-Martínez, J., *ChemCatChem*, 2014, **6**, 46-66.

22. A. Feliczak-Guzik, *Micropor. Mesopor. Mater.*, 2018, **259**, 33-45.
23. T.C. Keller, J. Arras, S. Wershofen, J. Pérez-Ramírez, *ACS Catal.*, 2015, **5**, 734-743.
24. C. Martínez, D. Verboekend, J. Pérez-Ramírez, A. Corma, A., *Catal. Sci. & Technol.*, 2013, **3**, 972-981.
25. M.S. Holm, E. Taarning, K. Egeblad, C.H. Christensen, *Catal. Today*, 2011, **168**, 3-16.
26. J.C. Groen, T. Sano, J.A. Moulijn, J. Pérez-Ramírez, *J. Catal.*, 2007, **251**, 21-27.
27. Y.-J. Lee, E.S. Kim, T.-W. Kim, C.-U. Kim, K.-E. Jeong, C.-H. Lee, S.-Y. Jeong, *J. Nanosci. Nanotechnol.*, 2015, **15**, 5334-5337.
28. S.-U. Lee, Y.-J. Lee, J.-R. Kim, E.-S. Kim, T.-W. Kim, H.J. Kim, C.-U. Kim, S.-Y. Jeong, *Mater. Res. Bull.*, 2017, **96**, 149-154.
29. C.A. Emeis, *J. Catal.*, 1993, **141**, 347-354.
30. G. Bergeret, P. Gallezot, *Handbook of Heterogeneous Catalysis*, 2008, 738-765.
31. C. Flego, N. Gigantiello, W.O. Parker, V. Calemma, *J. Chromatogr. A*, 2009, **1216**, 2891-2899.
32. S. Rabl, A. Haas, D. Santi, C. Flego, M. Ferrari, V. Calemma, J. Weitkamp, *Appl. Catal. A*, 2011, **400**, 131-141.
33. S. Rabl, D. Santi, A. Haas, M. Ferrari, V. Calemma,G. Bellussi, J. Weitkamp, *Micropor. Mesopor. Mater.*, 2011, **146**, 190-200.
34. D. Verboekend, G. Vilé, J. Pérez-Ramírez, *Adv. Funct. Mater.*, 2012, **22**, 916-928.
35. S. Fernandez, M.L. Ostraat, J.A. Lawrence, K. Zhang, *Micropor. Mesopor. Mater.*, 2018, **263**, 201-209.
36. I. Kiricsi, C. Flego, G. Pazzuconi, W.O. Parker, Jr., R. Millini, C. Perego, G. Bellussi, *J. Phys. Chem.*, 1994, **98**, 4627-34.
37. B.J. Kip, F.B.M. Duivenvoorden, D.C. Koningsberger, R. Prins, *J. Catal.*, 1987, **105**, 26-38.
38. G.B. McVicker, R.T.K. Baker, R.L. Garten, E.L. Kugler, *J. Catal.*, 1980, **65**, 207-220.
39. C.H. Bartholemew, in *Catalysis: Volume 11*, J.J. Spivey, S.K. Agarwal, Eds., The Royal Society of Chemistry, 1994, 93-126.
40. J. Freel, *J. Catal.*, 1972, **25**, 149-160.
41. D. Kubička, N. Kumar, P. Mäki-Arvela, M. Tiitta, V. Niemi, H. Karhu, T. Salmi, D.Y. Murzin, *J. Catal.*, 2004, **227**, 313-327.
42. C.A.A. Monteiro, D. Costa, J.L. Zotin, D. Cardoso, *Fuel*, 2015, **160**, 71-79.
43. W.-C. Lai, C. Song, *Catal. Today*, 1996, **31**, 171-181.
44. A. Haas, S. Rabl, M. Ferrari, V. Calemma, J. Weitkamp, *Appl. Catal. A*, 2012, **425-426**, 97-109.
45. R. Moraes, K. Thomas, S. Thomas, S. Van Donk, G. Grasso, J.-P. Gilson, M. Houalla, *J. Catal.*, 2012, **286**, 62-77.